LETTER

doi:10.1038/nature15723

Large anomalous Hall effect in a non-collinear antiferromagnet at room temperature

Satoru Nakatsuji[1,2], Naoki Kiyohara[1] & Tomoya Higo[1]

In ferromagnetic conductors, an electric current may induce a transverse voltage drop in zero applied magnetic field: this anomalous Hall effect[1] is observed to be proportional to magnetization, and thus is not usually seen in antiferromagnets in zero field[2]. Recent developments in theory and experiment have provided a framework for understanding the anomalous Hall effect using Berry-phase concepts[3], and this perspective has led to predictions that, under certain conditions, a large anomalous Hall effect may appear in spin liquids and antiferromagnets without net spin magnetization[4–8]. Although such a spontaneous Hall effect has now been observed in a spin liquid state[9], a zero-field anomalous Hall effect has hitherto not been reported for antiferromagnets. Here we report empirical evidence for a large anomalous Hall effect in an antiferromagnet that has vanishingly small magnetization. In particular, we find that Mn_3Sn, an antiferromagnet that has a non-collinear 120-degree spin order[10,11], exhibits a large anomalous Hall conductivity of around 20 per ohm per centimetre at room temperature and more than 100 per ohm per centimetre at low temperatures, reaching the same order of magnitude as in ferromagnetic metals[3]. Notably, the chiral antiferromagnetic state has a very weak and soft ferromagnetic moment of about 0.002 Bohr magnetons per Mn atom (refs 10, 12), allowing us to switch the sign of the Hall effect with a small magnetic field of around a few hundred oersted. This soft response of the large anomalous Hall effect could be useful for various applications including spintronics—for example, to develop a memory device that produces almost no perturbing stray fields.

Mn_3Sn is a hexagonal antiferromagnet (AFM) that exhibits non-collinear ordering of Mn magnetic moments at the Néel temperature of $T_N \approx 420$ K (refs 10, 11, 13). The system has a hexagonal Ni_3Sn-type structure with space group $P6_3/mmc$ (Fig. 1a). The structure is stable only in the presence of excess Mn, which randomly occupies the Sn site[13]. The basal plane projection of the Mn sublattice can be viewed as a triangular lattice arrangement of a twisted triangular tube made of face-sharing octahedra (Fig. 1a, b). Each a–b plane consists of a slightly distorted kagome lattice of Mn moments each of ~3 μ_B (where μ_B is the Bohr magneton), and the associated geometrical frustration manifests itself as an inverse triangular spin structure that carries a very small net ferromagnetic moment of ~0.002 μ_B per Mn atom (Fig. 1c)[10,11]. All Mn moments lie in the a–b plane and form a chiral spin texture with an opposite vector chirality to the usual 120° structure (Extended Data Fig. 1). This inverse triangular configuration has an orthorhombic symmetry, and only one of the three moments in each Mn triangle is parallel to the local easy-axis[10–12] (Fig. 1c). Thus, the canting of the other two spins towards the local easy-axis is considered to be the origin of the weak ferromagnetic moment[10–12].

It is known that as-grown crystals retain the inverse triangular spin state over a wide temperature (T) range between T_N and ~50 K (ref. 14). At low temperatures, a cluster glass phase appears with a large c-axis ferromagnetic component due to spin canting towards the c axis[11,15,16]. In this work, we used as-grown single crystals that have the composition $Mn_{3.02}Sn_{0.98}$ and confirmed no transition except the one at 50 K (Methods). As the detailed spin structure is unknown for the low temperature phase, here we focus on the phase stable above 50 K, and use 'Mn_3Sn' to refer to our crystals for clarity.

We first show our main experimental evidence for the large anomalous Hall effect (AHE) at room temperature. Figure 2a presents the field dependence of the Hall resistivity, $\rho_H(B)$, obtained at 300 K for the field along $[2\bar{1}\bar{1}0]$ (a axis). $\rho_H(B)$ exhibits a clear hysteresis loop with a sizable jump of $|\Delta\rho_H| \approx 6\ \mu\Omega$ cm. This is strikingly large for an AFM, and is larger than those found in elemental transition metal ferromagnets (FMs) such as Fe, Co and Ni (refs 2, 3, 17). Notably, the sign change occurs at a small field of ~300 Oe. Furthermore, the hysteresis remains sharp and narrow in all the temperature range between 100 K and 400 K (Fig. 2b). In this temperature region, a large anomaly as a function of field has been seen only in the Hall resistivity. The longitudinal resistivity $\rho(B)$ remains constant except for spikes at the critical fields where the Hall resistivity jumps (Fig. 2a).

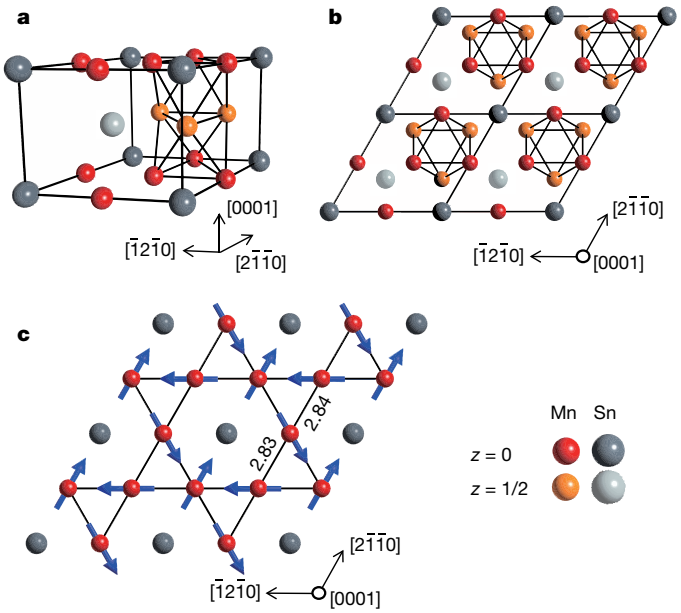

Figure 1 | Crystal and magnetic structures of Mn_3Sn. a, The crystallographic unit cell of Mn_3Sn. Although there is only one crystallographic site for both Mn and Sn, different colours are used to distinguish those in the $z = 0$ plane and in the $z = 1/2$ plane. In addition to the unit cell frame, Mn atoms are connected by lines to illustrate that the face-sharing octahedra of Mn atoms form a twisted triangular tube along the c axis. **b**, Top view along the c axis of the neighbouring four unit cells in the a–b plane. **c**, An individual a–b plane of Mn_3Sn. All distances are in Å. Mn moments (arrows) form an inverse triangular spin structure[10–12]. Each Mn moment has the local easy-axis parallel to the in-plane direction towards its nearest-neighbour Sn sites. Here, $[2\bar{1}\bar{1}0]$ and (0001) mean the a axis and the a–b plane, respectively.

[1]Institute for Solid State Physics, University of Tokyo, Kashiwa 277-8581, Japan. [2]PRESTO, Japan Science and Technology Agency (JST), 4-1-8 Honcho Kawaguchi, Saitama 332-0012, Japan.

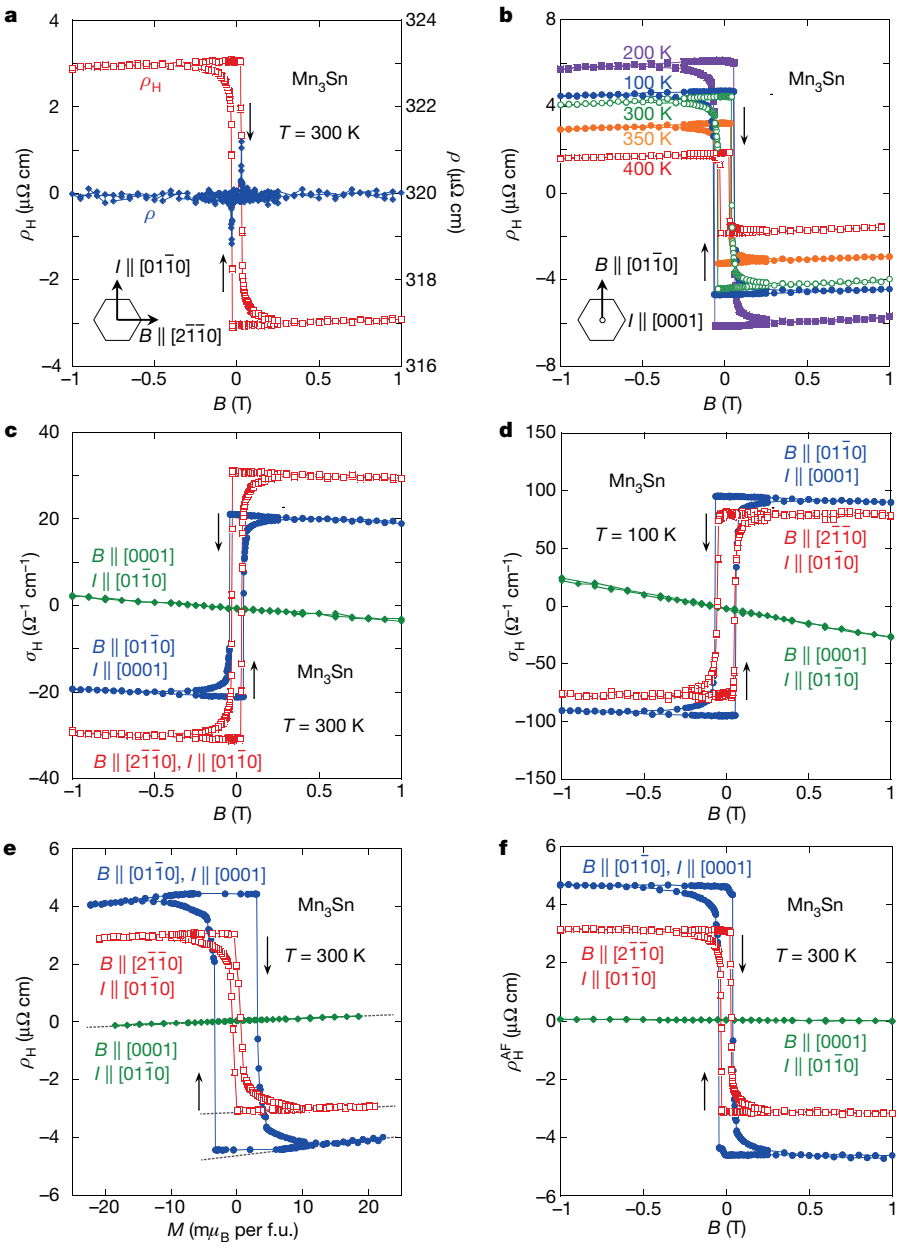

Figure 2 | Magnetic field dependence of the AHE in Mn_3Sn. a, Field dependence of the Hall resistivity ρ_H (left axis) and the longitudinal resistivity ρ (right axis) at 300 K in the magnetic field $B \parallel [2\bar{1}\bar{1}0]$ with the electric current $I \parallel [01\bar{1}0]$. **b**, Field dependence of the Hall resistivity ρ_H at various temperatures in $B \parallel [01\bar{1}0]$ with $I \parallel [0001]$. **c**, **d**, The Hall conductivity σ_H versus B measured in $B \parallel [2\bar{1}\bar{1}0]$, $[01\bar{1}0]$ and $[0001]$ obtained at 300 K (**c**) and 100 K (**d**). **e**, Magnetization dependence of ρ_H at 300 K. **f**, Field dependence of $\rho_H^{AF} = \rho_H - R_0 B - R_s \mu_0 M$ at 300 K. The arrows in the hexagon at lower left in **a** and **b** indicate the field and current directions in the hexagonal lattice of Mn_3Sn.

Correspondingly, the Hall conductivity, $\sigma_H = -\rho_H/\rho^2$, for in-plane fields along both $[2\bar{1}\bar{1}0]$ and $[01\bar{1}0]$ shows a large jump and narrow hysteresis (Fig. 2c, d). For instance, with $B \parallel [01\bar{1}0]$, σ_H has large values near zero field, ~20 Ω^{-1} cm^{-1} at 300 K and nearly 100 Ω^{-1} cm^{-1} at 100 K. This is again quite large for an AFM and comparable to those values found in ferromagnetic metals[3,17]. On the other hand, the Hall conductivity for $B \parallel [0001]$ (c axis) shows no hysteresis but only a linear field dependence.

The magnetization curve $M(B)$ shows anisotropic hysteresis similar to that found for the Hall effect. For example, M versus $B \parallel [01\bar{1}0]$ at temperatures between 100 K and 400 K shows a clear hysteresis, indicating that a weak ferromagnetic moment (4–7 mμ_B per formula unit (f.u.)) changes its direction with coercivity of only a few hundred oersted (Fig. 3a). Whereas the in-plane M is almost isotropic and has a narrow hysteresis, the magnetization shows only a linear dependence on B for $B \parallel [0001]$ at all the temperatures measured between 100 K and 450 K (Fig. 3b). The similar anisotropic and hysteretic behaviours found in both $\rho_H(B)$ and $M(B)$ indicate that the existence of the small and soft ferromagnetic component allows us to switch the sign of the Hall effect. Indeed, previous neutron diffraction measurements and theoretical analyses clarified that the inverse triangular spin structure has no in-plane anisotropy energy up to the fourth-order term[10,12], which is consistent with the observed small coercivity. This further indicates that by rotating the net ferromagnetic moment, one may switch the staggered moment direction of the triangular spin structure[10,12]. This switch should be the origin of the sign change of the Hall effect, as we discuss below. On heating, this ferromagnetic component vanishes at the Néel temperature of 430 K, above which the hysteresis disappears in both the T and B dependence of the magnetization (Fig. 3a and its inset).

To reveal the temperature evolution of the spontaneous component of the AHE, both the zero-field Hall resistivity $\rho_H(B=0)$ and the zero-field longitudinal resistivity $\rho(B=0)$ were measured after cooling samples in a magnetic field of $B_{FC} = 7$ T from 400 K down to 5 K and subsequently setting B to 0 at 5 K (Methods). Figure 4a shows the temperature dependence of the zero-field Hall conductivity $\sigma_H(B=0) = -\rho_H(B=0)/\rho^2(B=0)$ obtained after the above field-cooling (FC) procedure using three different configurations of the magnetic field (B_{FC}) and electric current (I) directions. Here, σ_{zx} stands for the Hall conductivity obtained after the FC procedure in $B_{FC} \parallel [01\bar{1}0]$ with $I \parallel [0001]$, and σ_{yz} for $B_{FC} \parallel [2\bar{1}\bar{1}0]$ and $I \parallel [01\bar{1}0]$. Both show large values at low temperatures, and in particular, $|\sigma_{zx}|$ exceeds 100 Ω^{-1} cm^{-1} at $T < 80$ K. Both $|\sigma_{zx}|$ and $|\sigma_{yz}|$ decrease on heating but still retain

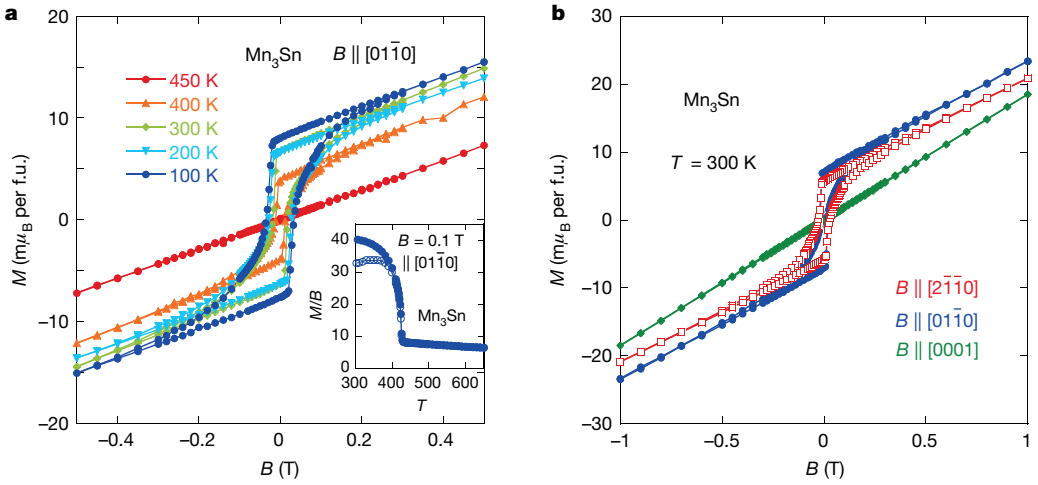

Figure 3 | In-plane weak ferromagnetism in Mn_3Sn. a, Field dependence of the magnetization M in the magnetic field $B \parallel [01\bar{1}0]$ at various temperatures. Inset shows the temperature (in K) dependence of the susceptibility M/B (in me.m.u. per mol per f.u.) obtained above 300 K in the field of 0.1 T $\parallel [01\bar{1}0]$. Filled and open symbols indicate the results obtained in the field-cooling and zero-field-cooling procedures, respectively (see Methods). **b**, Anisotropy in the magnetization curve obtained at 300 K in $B \parallel [2\bar{1}\bar{1}0]$, $[01\bar{1}0]$ and [0001].

values of ~10 Ω^{-1} cm^{-1} at 400 K, which is the highest temperature of our measurements. On the other hand, σ_{xy} obtained after the FC procedure in $B_{FC} \parallel [0001]$ with $I \parallel [01\bar{1}0]$ is zero within our experimental accuracy at $T > 50$ K. In the low temperature phase below 50 K, $|\sigma_{xy}|$ increases on cooling and reaches 140 Ω^{-1} cm^{-1} at 5 K, the lowest temperature of our measurements. In the three FC procedures described above, the temperature dependence of the longitudinal resistivity $\rho(B=0)$ was also concomitantly obtained (Fig. 4a, inset). Both in-plane and out-of-plane components show saturation at $T > 300$ K, indicating the presence of strong inelastic scattering at high temperatures.

Conventionally, the Hall resistivity is described as $\rho_H = R_0 B + R_s \mu_0 M$. Here, R_0 and R_s are the ordinary and anomalous Hall coefficients, and μ_0 is the permeability. To further examine the field and magnetization dependence of the AHE, we estimated the ordinary Hall contribution $R_0 B$ by using the temperature dependent ρ_H and M/B for $B \parallel c$ (Extended Data Fig. 2, Methods). The obtained $R_0 = 3.0 \times 10^{-4}$ cm^3 C^{-1} indicates that $R_0 B$ is negligibly small compared to the observed ρ_H. Plotting ρ_H versus M in Fig. 2e, we note that ρ_H for $B \parallel c$ has a normal M-linear AHE. Likewise, ρ_H for $B \parallel a$–b also shows an M-linear AHE in field, $\Delta\rho_H = R_s \mu_0 M$ (broken lines). Clearly, however, the large hysteresis with a sharp sign change in ρ_H cannot be described by the simple linear term, indicating that there is another dominant contribution to the AHE. If we label this additional term as ρ_H^{AF}, the Hall resistivity in Mn_3Sn can be described by

$$\rho_H = R_0 B + R_s \mu_0 M + \rho_H^{AF} \quad (1)$$

By subtracting $R_0 B$ and $R_s \mu_0 M$ from ρ_H, we find that ρ_H^{AF} is nearly independent of B or M, unlike what is found in FMs (Fig. 2f, Extended Data Fig. 3). With the reversal of a small applied field, ρ_H^{AF} changes sign, corresponding to the rotation of the staggered moments of the non-collinear spin structure[10,12]. Thus, the large AHE, ρ_H^{AF}, must have a distinct AF-driven origin.

In a magnetic conductor with relatively high resistivity, the AHE is dominated by contributions $\propto \rho^2$. Thus, it is useful to compare $S_H = \mu_0 R_s / \rho^2$ for Mn_3Sn with those for various magnets (Extended Data Table 1, Methods)[3]. Normally for FMs such as Fe, Ni and MnSi, S_H is known to be field-independent, and takes values of the order of 0.01–0.1 V^{-1} (refs 3, 18, 19). Indeed, the field-induced M-linear contribution of the AHE has a field-independent S_H, which has the positive sign and the same order of magnitude as in FMs. On the other hand, one can also define S_H for the spontaneous component at zero field as $S_H^0 = \rho_H(B=0)/[\rho^2(B=0)M(B=0)] = \rho_H^{AF}(B=0)/[\rho^2(B=0)M(B=0)] + S_H$. We find significantly large $|S_H^0| \gg |S_H|$, reaching 14 V^{-1} at 100 K and with a different sign from S_H (Fig. 4b, Extended Data Table 1). This indicates that ρ_H^{AF}, which is the dominant part of the spontaneous component, has a different origin from the conventional AHE (Methods).

A large AHE in a non-collinear AFM was first theoretically predicted for Mn_3Ir, which has a stacked kagome lattice of Mn atoms, similarly to Mn_3Sn (ref. 7). Chen *et al.*[7] considered that an AHE may be induced by breaking a symmetry of a single layer kagome lattice that has a triangular

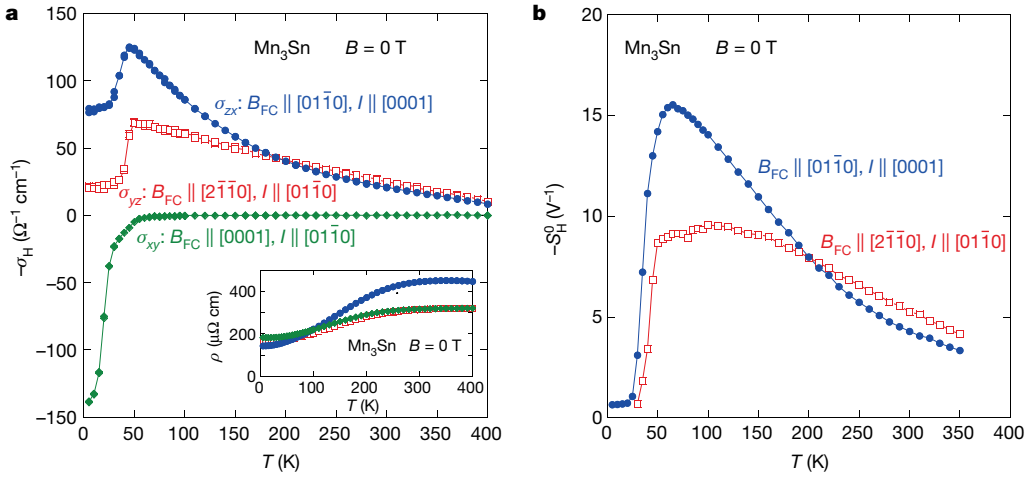

Figure 4 | Temperature evolution of the zero-field component of the AHE. Open square, filled circle and filled diamond symbols represent the results obtained after field-cooling (FC) procedures under magnetic field B_{FC} along the $[2\bar{1}\bar{1}0]$, $[01\bar{1}0]$ and [0001] directions, respectively. The directions of the electric current I are also specified in each main panel. For details, see Methods. **a**, Temperature dependence of the anomalous Hall conductivity, $\sigma_H(B=0)$. Inset, temperature dependence of the zero-field resistivity concomitantly obtained after the same FC procedures. **b**, Temperature dependence of $S_H^0 = -\sigma_H(B=0) / M(B=0)$ obtained after the FC procedures. Here $M(B=0)$ is the remanent magnetization.

magnetic order, and confirmed the large AHE by numerical calculations. Similar symmetry arguments apply to Mn_3Sn. In this case, the inverse triangular magnetic order breaks the in-plane hexagonal symmetry of the lattice, and thus may induce an AHE in the a–b plane. Indeed Kübler *et al.*[8] have theoretically found a large AHE in Mn_3Sn, calculating the anomalous Hall conductivity through the Brillouin zone integration of the Berry curvature[3,20]. Interestingly, they found a significant enhancement of the Berry curvature, particularly around band crossing points called Weyl points[21,22] near the Fermi energy. Experimental confirmation of the existence of the Weyl points (for example by ARPES measurements) is awaited. On the other hand, the observed $\sigma_{xy} = 0$ at $T > 50$ K is consistent with the in-plane coplanar spin structure and with the absence of a topological Hall effect due to spin chirality[4–6,8]. The large enhancement in $|\sigma_{xy}|$ at $T < 50$ K, however, may contain the topological Hall contribution as spins cant towards the c axis in the low-T phase. It would be interesting to verify this possibility in future studies.

Various applications are conceivable for the observed large AHE and its soft response to applied field. One possibility is for non-volatile memory. To date, FMs have been used as the main active materials for memory devices[23]. However, AFMs have recently attracted attention, because the small magnitude of their stray fields provides stability against magnetic field perturbations, opening new avenues to achieving high data retention and high-density memory integration[24–29]. In addition, AFMs have much faster spin dynamics than FMs, which may lead to ultrafast data processing[26,29].

To develop useful magnetic devices, one needs to find detectable macroscopic effects that are induced by the rotation of the order parameter. Such effects commonly used for FMs are often unavailable in AFMs as they have zero or vanishingly small magnetization. However, recent theoretical studies have proposed that such spin-axis change can be observed in AFMs[24–26,29]—for instance, through anisotropic magnetoresistance (AMR) effects[25]. Experimental demonstrations have been performed at room temperature in which rotation of AF moments was detected as the AMR changed by a few tens of milliohms, which is of the order of 0.1% of the total resistance[28].

The AHE provides another useful probe for the spin-axis switch, and therefore may serve as an electrical means for reading magnetically stored information. In fact, in Mn_3Sn the Hall voltage can be readily detected as it generates a sizeable resistance jump at room temperature (for example, >500 mΩ for a 100-nm-thick thin film and $|\Delta\rho_H|/\rho > 1\%$) and this material has no magnetoresistance up to several tesla. Thus, the sharp Hall resistance change can be easily tuned to be more than 10% of the total resistance by reducing the misalignment of Hall voltage contacts.

Whereas the remanent magnetization and thus stray fields of Mn_3Sn should be two to three orders of magnitude smaller than in ordinary FMs, its coercivity of a few hundred oersted is close to that of FMs used in magnetic devices. It will therefore be interesting to explore the possibility of using electrical means not only for reading but also for writing information—for example, by spin transfer torque[24,26,29]. Finally, we note that the present exceptionally large AHE found in an AFM with vanishingly small magnetization indicates that a large fictitious field due to Berry phase must exist in momentum space, and is expected to generate various effects including orbital ferromagnetism[4,20] and the spin Hall effect[30]. Exploration of such effects and their external-field control are suitable subjects for future studies.

Online Content Methods, along with any additional Extended Data display items and Source Data, are available in the online version of the paper; references unique to these sections appear only in the online paper.

Received 3 May; accepted 1 September 2015.
Published online 28 October 2015.

1. Hall, E. H. On the "rotational coefficient" in nickel and cobalt. *Proc. Phys. Soc. Lond.* **4,** 325–342 (1880).
2. Chien, C. L. & Westgate, C. R. *The Hall Effect and its Applications* (Plenum, 1980).
3. Nagaosa, N., Sinova, J., Onoda, S., MacDonald, A. H. & Ong, N. P. Anomalous Hall effect. *Rev. Mod. Phys.* **82,** 1539–1592 (2010).
4. Shindou, R. & Nagaosa, N. Orbital ferromagnetism and anomalous Hall effect in antiferromagnets on the distorted fcc lattice. *Phys. Rev. Lett.* **87,** 116801 (2001).
5. Metalidis, G. & Bruno, P. Topological Hall effect studied in simple models. *Phys. Rev. B* **74,** 045327 (2006).
6. Martin, I. & Batista, C. D. Itinerant electron-driven chiral magnetic ordering and spontaneous quantum Hall effect in triangular lattice models. *Phys. Rev. Lett.* **101,** 156402 (2008).
7. Chen, H., Niu, Q. & MacDonald, A. H. Anomalous Hall effect arising from noncollinear antiferromagnetism. *Phys. Rev. Lett.* **112,** 017205 (2014).
8. Kübler, J. & Felser, C. Non-collinear antiferromagnets and the anomalous Hall effect. *Europhys. Lett.* **108,** 67001 (2014).
9. Machida, Y., Nakatsuji, S., Onoda, S., Tayama, T. & Sakakibara, T. Time-reversal symmetry breaking and spontaneous Hall effect without magnetic dipole order. *Nature* **463,** 210–213 (2010).
10. Tomiyoshi, S. & Yamaguchi, Y. Magnetic structure and weak ferromagnetism of Mn_3Sn studied by polarized neutron diffraction. *J. Phys. Soc. Jpn* **51,** 2478–2486 (1982).
11. Brown, P. J., Nunez, V., Tasset, F., Forsyth, J. B. & Radhakrishna, P. Determination of the magnetic structure of Mn_3Sn using generalized neutron polarization analysis. *J. Phys. Condens. Matter* **2,** 9409–9422 (1990).
12. Nagamiya, T., Tomiyoshi, S. & Yamaguchi, Y. Triangular spin configuration and weak ferromagnetism of Mn_3Sn and Mn_3Ge. *Solid State Commun.* **42,** 385–388 (1982).
13. Krén, E., Paitz, J., Zimmer, G. & Zsoldos, É. Study of the magnetic phase transformation in the Mn_3Sn phase. *Physica B* **80,** 226–230 (1975).
14. Ohmori, H., Tomiyoshi, S., Yamauchi, H. & Yamamoto, H. Spin structure and weak ferromagnetism of Mn_3Sn. *J. Magn. Magn. Mater.* **70,** 249–251 (1987).
15. Tomiyoshi, S., Abe, S., Yamaguchi, Y., Yamauchi, H. & Yamamoto, H. Triangular spin structure and weak ferromagnetism of Mn_3Sn at low temperature. *J. Magn. Magn. Mater.* **54–57,** 1001–1002 (1986).
16. Feng, W. J. *et al.* Glassy ferromagnetism in Ni_3Sn-type $Mn_{3.1}Sn_{0.9}$. *Phys. Rev. B* **73,** 205105 (2006).
17. Miyasato, T. *et al.* Crossover behavior of the anomalous Hall effect and anomalous Nernst effect in itinerant ferromagnets. *Phys. Rev. Lett.* **99,** 086602 (2007).
18. Neubauer, A., Pfleiderer, C., Ritz, R., Niklowitz, P. G. & Böni, P. Hall effect and magnetoresistance in MnSi. *Physica B* **404,** 3163–3166 (2009).
19. Manyala, N. *et al.* Large anomalous Hall effect in a silicon-based magnetic semiconductor. *Nature Mater.* **3,** 255–262 (2004).
20. Xiao, D., Chang, M.-C. & Niu, Q. Berry phase effects on electronic properties. *Rev. Mod. Phys.* **82,** 1959–2007 (2010).
21. Wan, X., Turner, A. M., Vishwanath, A. & Savrasov, S. Y. Topological semimetal and Fermi-arc surface states in the electronic structure of pyrochlore iridates. *Phys. Rev. B* **83,** 205101 (2011).
22. Burkov, A. A. & Balents, L. Weyl semimetal in a topological insulator multilayer. *Phys. Rev. Lett.* **107,** 127205 (2011).
23. Chappert, C., Fert, A. & Nguyen Van Dau, F. The emergence of spin electronics in data storage. *Nature Mater.* **6,** 813–823 (2007).
24. Núñez, A. S., Duine, R. A., Haney, P. & MacDonald, A. H. Theory of spin torques and giant magnetoresistance in antiferromagnetic metals. *Phys. Rev. B* **73,** 214426 (2006).
25. Shick, A. B., Khmelevskyi, S., Mryasov, O. N., Wunderlich, J. & Jungwirth, T. Spin-orbit coupling induced anisotropy effects in bimetallic antiferromagnets: a route towards antiferromagnetic spintronics. *Phys. Rev. B* **81,** 212409 (2010).
26. MacDonald, A. H. & Tsoi, M. Antiferromagnetic metal spintronics. *Phil. Trans. R. Soc. A* **369,** 3098–3114 (2011).
27. Park, B. G. *et al.* A spin-valve-like magnetoresistance of an antiferromagnet-based tunnel junction. *Nature Mater.* **10,** 347–351 (2011).
28. Marti, X. *et al.* Room-temperature antiferromagnetic memory resistor. *Nature Mater.* **13,** 367–374 (2014).
29. Gomonay, E. V. & Loktev, V. M. Spintronics of antiferromagnetic systems. *Low Temp. Phys.* **40,** 17–35 (2014).
30. Hirsch, J. E. Spin Hall effect. *Phys. Rev. Lett.* **83,** 1834–1837 (1999).

Acknowledgements We thank M. Ikhlas and A. Nevidomskyy for discussions. This work was partially supported by PRESTO, by the Japan Science and Technology Agency, by Grants-in-Aid for Scientific Research (no. 25707030) and the Program for Advancing Strategic International Networks to Accelerate the Circulation of Talented Researchers (no. R2604), and by Grants-in-Aid for Scientific Research on Innovative Areas (15H05882, 15H05883) from the Japanese Society for the Promotion of Science. The use of the facilities of the Materials Design and Characterization Laboratory at the Institute for Solid State Physics, The University of Tokyo, is acknowledged.

Author Contributions S.N. planned the experimental project, and S.N. and N.K. performed experiments and collected data. S.N., N.K. and T.H. wrote the paper and prepared figures; all authors discussed the results and commented on the manuscript.

Author Information Reprints and permissions information is available at www.nature.com/reprints. The authors declare no competing financial interests. Readers are welcome to comment on the online version of the paper. Correspondence and requests for materials should be addressed to S.N. (satoru@issp.u-tokyo.ac.jp).

METHODS

Polycrystalline samples were prepared by arc-melting mixtures of manganese and tin in a purified argon atmosphere. Excess manganese (10 mol%) over the stoichiometric amount was added to compensate for loss during arc-melting and single-crystal growth. The polycrystalline materials obtained were used to grow single crystals by the Czochralski method, using a commercial tetra-arc furnace (TAC-5100, GES). Our single-crystal and powder X-ray measurements indicate a single phase of hexagonal Mn_3Sn with lattice constants of $a = 5.66(1)$ Å and $c = 4.53(1)$ Å. Our scanning electron microscopy-energy dispersive X-ray analysis confirmed that Mn_3Sn is the bulk phase, and analysis using inductively coupled plasma spectroscopy found that the composition of the single crystals is $Mn_{3.02}Sn_{0.98}$.

For measurements of resistivity and magnetization, we used as-grown single crystals fashioned into bar-shaped samples after alignment using a Laue diffractometer. For our crystals, no annealing was performed below 800 °C, and thus the triangular spin configuration remains stable at least down to 50 K, below which the spins cant slightly towards the c axis[11,14,15].

Magnetization measurements were made using a commercial SQUID magnetometer (MPMS, Quantum Design). Both longitudinal and Hall resistivities were measured by a standard four-probe method using a commercial system (PPMS, Quantum Design). The field dependence of the Hall resistivity was obtained after subtracting the longitudinal resistivity component, which is found to be constant as a function of the magnetic field.

The zero-field component of the AHE shown in Fig. 4 was estimated by the following method. We cooled samples from 400 K down to 5 K under a field of $B_{FC} = 7\,T(-7\,T)$, and subsequently at 5 K we decreased the field B down to $+0\,T$ $(-0\,T)$ without changing the sign of B. (Here we use $+0$ and -0 to indicate zero approached from the positive side and negative side, respectively.) Then, we measured the Hall voltage $V_H(B\rightarrow+0)(V_H(B\rightarrow-0))$ in zero field after heating to various temperatures, stabilizing the temperature at each point. To remove the longitudinal resistance component due to the misalignment of the Hall voltage contacts, we estimated the zero-field component of the Hall resistance as $R_H(B=0) = [V_H(B\rightarrow+0) - V_H(B\rightarrow-0)]/2I$, where I is the electric current. Three different samples were used for the three different field-cooling configurations shown in Fig. 4. The longitudinal resistivity at zero field $\rho(B=0)$ was measured concomitantly in the same procedures as those used for the Hall resistivity measurements. The zero-field remanent magnetization $M(B=0)$ was also measured using the same field-cooling procedures as used in both longitudinal and Hall resistivity measurements.

As discussed in the main text, the Hall resistivity in Mn_3Sn can be described by equation (1). The unconventional AHE term ρ_H^{AF} due to the non-collinear AF spin structure appears only in the a–b plane components, and is absent when $B \parallel c$. Thus, to estimate the ordinary Hall coefficient, we measured the temperature dependence of the c-axis components of both the Hall resistivity ρ_H and the susceptibility $\chi = M/B$ under $B = 0.1\,T \parallel c$ (Extended Data Fig. 2a, b). Extended Data Figure 2c shows the Hall coefficient $R_H = \rho_H/B$ versus the susceptibility M/B. A good fit using equation (1) with $\rho_H^{AF} = 0$ was obtained for a wide range of temperature between 50 K and 300 K. The fitting yields $R_0 = 3.0 \times 10^{-4}\,cm^3C^{-1}$, which corresponds to a carrier concentration of $1.9 \times 10^{22}\,cm^{-3}$. $R_S = 0.86\ cm^3\ C^{-1}$ obtained by the fitting is consistent with another estimate at 300 K of $R_S = 0.5\,cm^3C^{-1}$, which is obtained by using the slope of the isothermal curve of ρ_H versus M in $B \parallel c$ (Fig. 2e). As $|R_S| \gg |R_0|$, the AHE dominates the Hall resistivity ρ_H, and the ordinary Hall contribution is negligibly small.

In magnetic conductors with relatively large resistivity, the AHE is dominated by contributions proportional to the resistivity squared, ρ^2, and thus it is useful to compare values of $S_H = \mu_0 R_s/\rho^2$ (ref. 3) obtained from different magnetic materials. Extended Data Table 1 shows a list of magnets that show an AHE whose dominant contribution is proportional to ρ^2, including Fe, Ni, the helimagnet MnSi and the dilute magnetic semiconductor $Ga_{1-x}Mn_xAs$ (refs 18, 19, 31–35). For comparison, we include in the list the non-collinear AFM Mn_5Si_3 (ref. 36).

$S_H^0 = -\sigma_H(B=0)\,/\,M(B=0)$ estimated at zero field for Mn_3Sn using the isothermal curves in Figs 2 and 3 reaches $-8.3\,V^{-1}$ (at 100 K), which is several orders of magnitude larger than in FMs such as Fe, Ni and MnSi (Extended Data Table 1). It is also much larger than the value for the non-collinear AFM Mn_5Si_3 with $T_N = 66$ K, which exhibits an AHE only by application of a magnetic field and thus has $\rho_H^{AF} = 0$ (ref. 36). To further estimate the temperature dependence of S_H^0, we measured the remanent magnetization $M(B=0)$ using the same FC procedures as used for the estimate of $\sigma_H(B=0)$. Figure 4b shows the temperature dependence of $S_H^0 = -\sigma_H(B=0)\,/\,M(B=0)$ for Mn_3Sn. Again in comparison with S_H known for metallic FMs (Extended Data Table 1), $S_H^0 \approx \rho_H^{AF}(B=0)\,/\left[\rho^2(B=0)M(B=0)\right]$ is larger by a factor of >10 and reaches $-14\,V^{-1}$ at 100 K.

On the other hand, in a magnetic field, both the in-plane and c-axis components of ρ_H have the M-linear AHE contribution, namely, $S_H\rho^2M$, as shown in Fig. 2e (broken lines). As $\rho(B)$ remains constant with field, S_H estimated using this field-induced M-linear contribution is also constant with field: the S_H we obtain is much smaller than, and has a different sign from, S_H^0. Interestingly, they are found to be roughly isotropic, and have the same order of magnitude as found in itinerant FMs (Extended Data Table 1). The fact that S_H^0 has a much larger value than, and a different sign from, S_H indicates that ρ_H^{AF} has a different origin from the conventional AHE, which is proportional to the magnetization.

To estimate ρ_H^{AF}, we subtracted the ordinary Hall effect R_0B and the M-linear term $S_H\rho^2M$ from the isothermal curve of ρ_H by using the above estimates of both R_0 and S_H. Note that the hysteresis in $M(B)$ was also taken into account for this subtraction. Interestingly, the isothermal curve of ρ_H^{AF} is nearly independent of either B or M, and shows a clear sign change with a hysteresis when the staggered moment direction of the non-collinear spin structure is switched by rotating the small net ferromagnetic moment[10,12] (Fig. 2f, Extended Data Fig. 3). This indicates that the large zero-field AHE, ρ_H^{AF}, comes from the non-collinear antiferromagnetism and is most probably driven by its Berry curvature effects.

31. Dheer, P. N. Galvanomagnetic effects in iron whiskers. *Phys. Rev.* **156,** 637–644 (1967).
32. Jan, J.-P. & Gijsman, H. M. L'effet Hall du fer et du nickel aux basses températures. *Physica* **18,** 339–355 (1952).
33. Husmann, A. & Singh, L. J. Temperature dependence of the anomalous Hall conductivity in the Heusler alloy Co_2CrAl. *Phys. Rev. B* **73,** 172417 (2006).
34. Chun, S. H. *et al.* Interplay between carrier and impurity concentrations in annealed $Ga_{1-x}Mn_xAs$: intrinsic anomalous Hall effect. *Phys. Rev. Lett.* **98,** 026601 (2007).
35. Onose, Y. & Tokura, Y. Doping dependence of the anomalous Hall effect in $La_{1-x}Sr_xCoO_3$. *Phys. Rev. B* **73,** 174421 (2006).
36. Sürgers, C., Fischer, G., Winkel, P. & v. Löhneysen, H. Large topological Hall effect in the non-collinear phase of an antiferromagnet. *Nature Commun.* **5,** 3400 (2014).

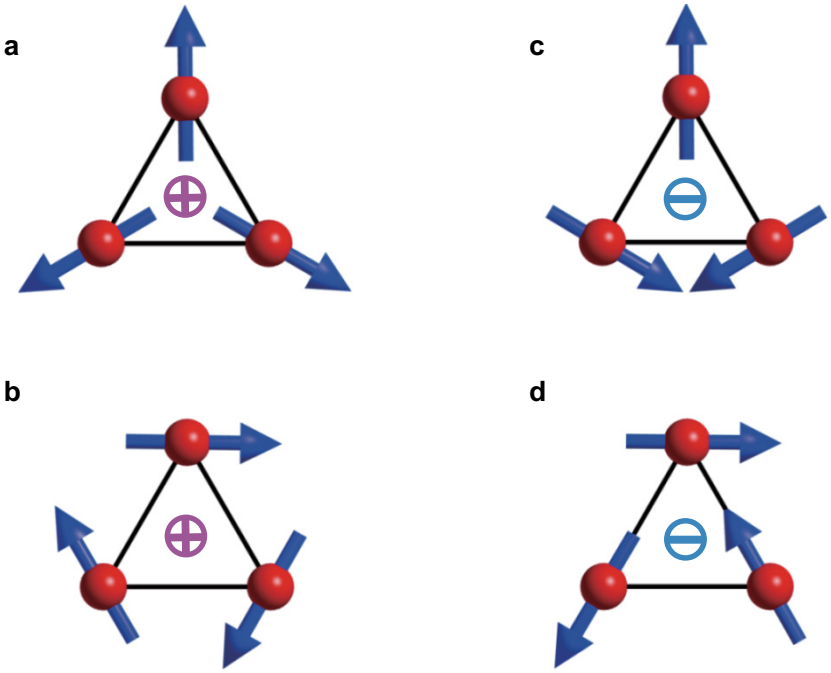

Extended Data Figure 1 | Normal and inverse triangular spin structures. **a**–**d**, Examples of normal (**a**, **b**) and inverse (**c**, **d**) triangular spin structures. An inverse triangular spin structure has the opposite sign of the vector spin chirality to a normal one. As each Mn moment has the local easy-axis parallel to the direction towards its in-plane nearest-neighbour Sn sites, the case shown in **d** is realized in Mn_3Sn (refs 10–12).

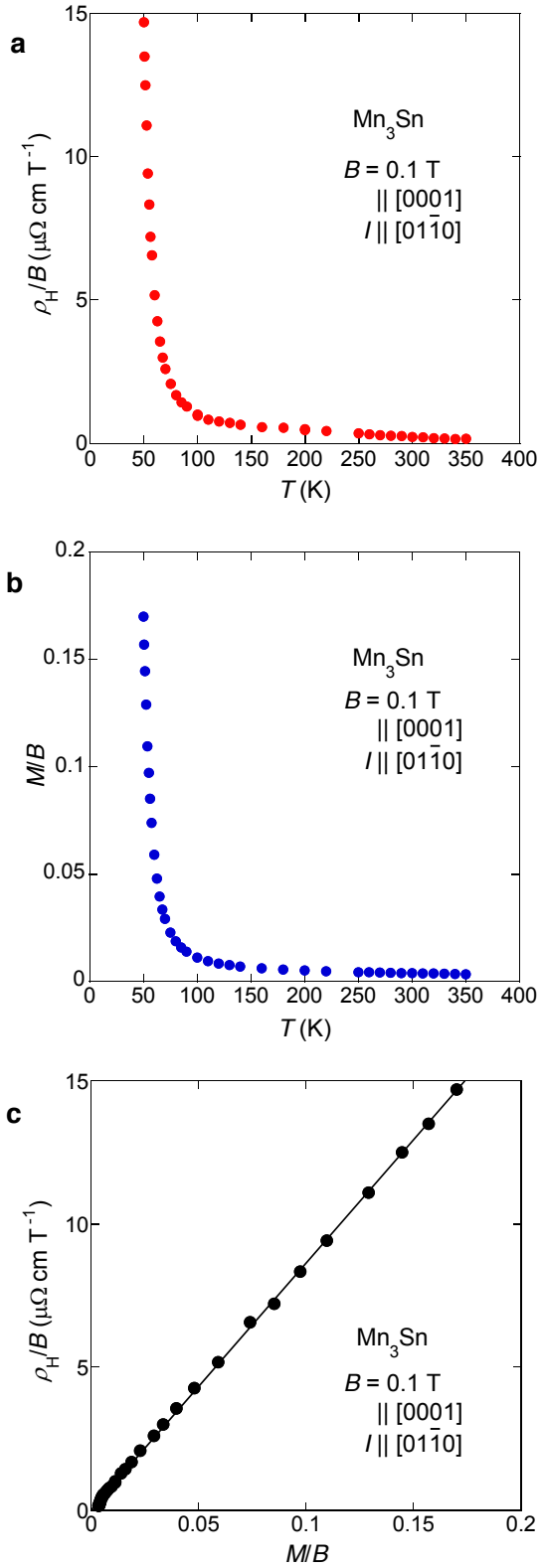

Extended Data Figure 2 | Estimation of the ordinary Hall effect using the *c*-axis components of the Hall resistivity. a, **b**, Temperature dependence of the Hall resistivity divided by B, ρ_H/B (**a**), and the susceptibility M/B obtained under a field of 0.1 T along the c axis (**b**). Measurements were made above $T = 50$ K, where no spontaneous components were observed. **c**, Plot of ρ_H/B versus M/B; here the temperature is an implicit parameter. The solid line indicates a linear fit to equation (1), with $\rho_H^{AF} = 0$ defined in Methods.

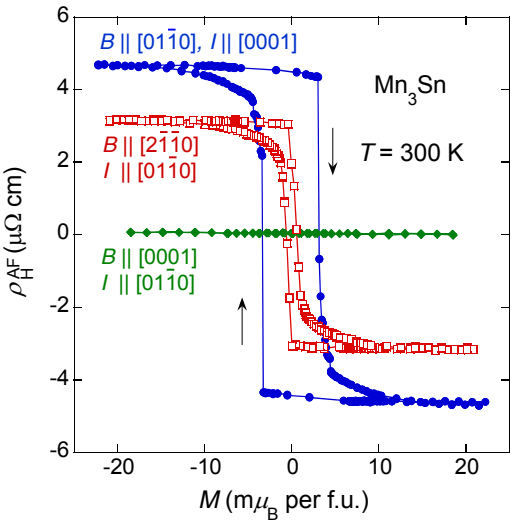

Extended Data Figure 3 | Magnetization dependence of the AF-driven Hall effect. Figure shows anisotropic isothermal curves of ρ_H^{AF} as a function of M at 300 K.

Extended Data Table 1 | Hall effect parameters for ferromagnets and antiferromagnets

Material	T [K]	n [10^{22} cm^{-3}]	S_H^0 [V^{-1}]	S_H [V^{-1}]	Reference
Mn_3Sn (AF)					
$B \parallel [01\bar{1}0]$, $I \parallel [0001]$	100	+1.9	−8.3	0.24	This work
$B \parallel [01\bar{1}0]$, $I \parallel [0001]$	300	+1.9	−2.2	0.069	This work
$B \parallel [2\bar{1}\bar{1}0]$, $I \parallel [01\bar{1}0]$	300	+1.9	−3.6	0.085	This work
$B \parallel [0001]$, $I \parallel [01\bar{1}0]$	300	+1.9		0.1	This work
Fe(bcc) (FM) ($B \parallel [100]$)	298	+34		0.06	Ref. 31
Ni (FM)	293	−11		−0.14	Ref. 32
MnSi (FM)	≤ 29.5	+5.9 – +8.5		−0.19	Ref. 18
$Fe_{1-x}Co_xSi$ (FM)	≤ 53	−0.26 – −0.10		0.022	Ref. 19
Co_2CrAl (FM)	36 – 278	> 0.03		0.039	Ref. 33
$Ga_{1-x}Mn_xAs$ (FM)	15	+0.01 – +0.09		0.04 – 0.06	Ref. 34
$La_{0.7}Sr_{0.3}CoO_3$ (FM)	2	+6		0.06	Ref. 35
$Mn_5Si_3C_{0.8}$ (FM)	100	+3		0.013	Ref. 36
Mn_5Si_3 (AF)	20	+0.3		−0.009	Ref. 36

Temperature (T), effective carrier density (n) and the coefficient S_H of the AHE are shown for various magnets. Here S_H is mostly determined by using the isothermal data of the Hall resistivity, magnetoresistivity and magnetization. For Mn_3Sn, two types of S_H are shown, namely, S_H for the AHE component that is linear in M, and S_H^0 for the zero-field spontaneous component of ρ_H (Methods). The sign of n indicates the type of carriers, namely, hole (+) or electron (−). Field (B) and current (I) direction are specified for some cases. AF, antiferromagnet; FM, ferromagnet; bcc, body-centred cubic. Data are from this work, and refs 18, 19, 31–36.